Published in final edited form as:
Chem Biol. 2014 June 19; 21(6): 775–781. doi:10.1016/j.chembiol.2014.05.007.

Folded Small Molecule Manipulation of Islet Amyloid Polypeptide

Sunil Kumar, **Mark A. Brown**, **Abhinav Nath**, and **Andrew D. Miranker***
Department of Molecular Biophysics and Biochemistry, Yale University, 260 Whitney Avenue, New Haven, CT 06520-8114

SUMMARY

Islet amyloid polypeptide (IAPP) is a hormone co-secreted with insulin by pancreatic β-cells. Upon contact with lipid bilayers, it is stabilized into a heterogeneous ensemble of structural states. These processes are associated with gains-of-function including catalysis of β-sheet rich amyloid formation, cell membrane penetration, loss of membrane integrity and cytotoxicity. These contribute to the dysfunction of β-cells, a central component in the pathology and treatment of diabetes. To gain mechanistic insight into these phenomena, a related series of substituted oligoquinolines were designed. These inhibitors are unique in that they have the capacity to affect both solution and phospholipid bilayer catalyzed IAPP self-assembly. Importantly, we show this activity is associated with the oligoquinoline's capacity to irreversibly adopt a non-covalently fold. This suggests that compact foldamer scaffolds, such as oligoquinoline, are an important paradigm for conformational manipulation of disordered protein states.

INTRODUCTION

The aggregation of proteins is implicated in the pathology of numerous diseases(Buxbaum, and Linke, 2012). For example, amyloid-β, α-synuclein, and IAPP underpin pathology in Alzheimers's disease (AD), Parkinson's disease, and type 2 diabetes respectively(Hebda, and Miranker, 2009). Proteins specific to these disorders undergo a conformational change from disordered to a cross-β sheet rich state. Transient intermediates of this process are associated with the toxic gains of function that define disease pathology.

Membrane-bound oligomeric intermediates of the amylodogenic protein IAPP are hypothesized to contribute to β-cell pathology in diabetes(Haataja, Gurlo, et al, 2008) as well as disease progression in AD(Walsh, Klyubin, et al, 2002) and Parkinson's(Winner,

Voice: (203) 432-8954, Fax: (203) 432-5175, andrew.miranker@yale.edu.

SUPPLEMENTAL INFORMATION
Supplemental information includes 34 figures (six figures are related to biophysical assays and 28 figures are related to the synthesis and characterization of oligoquinolines), two schemes, and one table. The supplemental information also includes general procedure for the synthesis of oligoquinolines.

Jappelli, et al, 2011). Such oligomers additionally display cell-penetration and mitochondrial dysfunction gains-of-function(Magzoub, and Miranker, 2012), which may account for data suggesting an intracellular location for toxic potential(Gurlo, Ryazantsev, et al, 2010). Small molecule approaches have been employed to probe the pathways of IAPP self-assembly. One approach is protein mimetics which can serve as template to match IAPP:IAPP, helix:helix interactions and thereby obstruct protein:protein interactions(Cummings, and Hamilton, 2010). Indeed, several compounds have been identified that bind to a membrane stabilized, α-helical sub-domain of IAPP(Hebda, Saraogi, et al, 2009). The scaffold, based on oligopyridine (OP) (Fig. 1A), was designed to project chemical moieties in a linear fashion with spacing that corresponds to the rise per turn of an α-helix. Here, we have taken an alternative approach in which a scaffold based on oligoquinoline (OQ) is used instead with the intended goal of it binding and acting as a perturbant of the target protein structure (Kumar, and Miranker, 2013). In essence, we are comparing the capacity of a foldamer versus a mimetic to affect the activity of an intrinsically disordered system.

The goal in foldamer design is to recapitulate properties evident in proteins(Gellman, 1998). Namely, the small molecule should cooperatively fold, have a defined and hierarchical structure, and be formed from a discrete length polymer capable of variation without affecting the first two properties. OQs have these properties and present alternative functional groups with a density that does not mimic an α-helix. We hypothesize that display of comparable moieties on OQ versus OP would create a state requiring a bound IAPP to change conformation. The size of the change in IAPP is unimportant except in the requirement that it be sufficient to affect its capacity to self-assemble. The role of structure formation by OQ and the molecular mechanism of perturbation of IAPPs gains of function are directly evaluated in this work.

RESULTS

A series of oligoquinolines (Fig. 1), were synthesized and used to make direct comparisons to oligopyridine scaffolds previously reported by us for the inhibition of membrane-catalyzed IAPP self-assembly(Hebda, Saraogi, et al, 2009). The pentameric oligoquinoline, OQ_5, inhibits large unilamellar vesicle (LUV) catalyzed conversion of IAPP to a β-sheet rich state. Upon exposure to 630 μM LUVs formed from a 1:1 mixture of anionic [dioleoylphosphatidylglycerol (DOPG)] and zwitterionic [dioleoylphosphatidylcholine (DOPC)] lipids, 30 μM IAPP undergoes a transition from a predominantly random coil conformation to one that includes strong spectroscopic contributions from α-helical structures (Fig. 2A). After ~1 hour, the protein converts to β-sheet rich species evident by a single Cotton effect minimum near ~218 nm. The presence of equimolar OQ_5 prohibits this conversion with α-helical states still dominant after 2 hr (Fig. 2A, S6). Imaging studies further show filamentous aggregate end-products, but only for reactions conducted in the absence of OQ_5 (Fig. 2B, C). The presence of OQ_5 plainly results in the delayed conversion of IAPP to a filamentous β-sheet rich state without diminishing the sampling of α-helical conformations.

Lipid catalyzed IAPP fibrillation is more inhibited by OQ_5 than by OP_5. Reactions were initiated by dilution of a 1 mM stock solution of IAPP into a standard buffer (see Materials

and Methods). Changes in fluorescence intensity of an exogenously added fluorophore, thioflavin T (ThT) allowed for real-time monitoring of the fibrillation(Wolfe, Calabrese, et al, 2010). Under these conditions, conversion of 10 μM IAPP to an aggregated state occurs with a reaction time midpoint (t_{50}) of 22±2 hr. In contrast, fibrillation is strongly accelerated by the presence LUVs (Fig. 2D). The t_{50} for 10 μM IAPP catalyzed by LUVs is 1.0±0.1 hr, consistent with our previously published reports(Hebda, Saraogi, et al, 2009). Addition of 100 μM OP_5 to an otherwise matched reaction results in inhibition of aggregation t_{50} by a factor of ~3 (Fig. 2D). Addition instead of 100 μM OQ_5 resulted in no detection of fibers. Using light scatter instead of ThT gave comparable results (Supporting Information Fig. S1 and Fig. S3). OQ_5 is plainly a more potent inhibitor of lipid catalyzed fiber formation than OP_5.

Reaction inhibition is sensitive to the repeat number of the mimetic subunit. For both the OP and OQ compound series, inhibition increases with increasing length (n=1–5) (Fig. 2E). The effect of OP compounds saturate at n=4–5 and display inhibition of 3–4 fold at an OP:IAPP ratio of 10:1. In contrast, OQ compounds do not behave methodically for n<5. At n=5, inhibition is abruptly complete (i.e. >20 hr). Lowering the small molecule:IAPP ratio to 1:1 exaggerates this observation with only OQ_5 showing any apparent inhibition (Fig. 2F).

Oligoquinolines affect IAPP via a mechanism that is distinct from oligopyridyls. IAPP self-assembly was observed under buffer only conditions (no LUVs). At 40 μM IAPP, the t_{50} for IAPP fibrillation is 1.9±0.1 hr (Fig. 3A). The presence of equimolar OP_5 instead results in a t_{50} of 1.1±0.1 hr, i.e. OP_5 is a mild agonist under bilayer-free conditions. In contrast, OQ_5 is a strong inhibitor. At a ratio of only 10:1, (IAPP:OQ_5) 3–4 fold inhibition is apparent (Fig. 3A). At 1:1, no conversion is apparent, even after 22 hr. Observations using light scatter, CD and TEM imaging give comparable results (Supporting Information Fig. S1). In part, these observations can be a consequence of OQ_5 effects on fiber elongation. In the presence of LUVs, a 10 μM reaction of IAPP is accelerated 5–6 fold by the addition of 0.1 μM IAPP as preformed fibers. One equivalent of OQ_5 is sufficient to negate this acceleration while 10 equivalents eliminates fiber formation (Supporting Information Fig. S4A). Similarly, in the absence of a bilayer catalyst, 0.1 equivalent of OQ_5 is sufficient to negate seeded acceleration (Supporting Information Fig. S4B). This stands in marked contrast to OP_5 in which 1 equivalent of small molecule is shown to have little effect on seeded reactions(Hebda, Saraogi, et al, 2009). Thus, under matched conditions, OP_5 is either neutral or acts as an agonist while OQ_5 acts as a potent antagonist.

Numerous small molecules have previously been reported as inhibitors of IAPP fiber formation. Here, we assess epigallocatechin-3-gallate (EGCG) and acid fuchsin. EGCG inhibits amyloid formation of many proteins including α-synuclein and Aβ-peptide and is currently under phase 2 clinical trials for Alzheimer's disease(Bieschke, Russ, et al, 2010). These molecules show significant (3–4 fold) inhibitory capacity in the absence of bilayer at equimolar protein:compound ratio (Fig. 3B). For both compounds however, no inhibition of IAPP assembly is apparent for lipid catalyzed fibrillation. To our knowledge OQ_5 is the first reported inhibitor of IAPP that functions effectively under both solution phase and lipid bilayer catalyzed conditions.

OQ_5 binds to the α-helical sub-domain of IAPP. OQ_5 was titrated into a solution of ^{15}N rIAPP and assessed for structural changes by NMR (Fig. 4A). Because of hIAPP's amyloidogenic nature under the NMR conditions, a sequence variant of IAPP from rodents (rIAPP) was used. We have previously shown that disruption of β-sheet formation strongly diminishes cytotoxic potential using rIAPP and its helical subdomain variant (H18R). This result has been recently confirmed(Cao, Abedini, et al, 2013). Importantly, elevation of peptide concentration to 200 and 50 μM respectively not only results in the restoration of colorimetrically assessed toxicity, but also a concentration dependent mitochondrial localization phenotype(Magzoub, and Miranker, 2012). By NMR, the residues affected by OQ_5, 3–20 (Fig. 4B), have been previously identified by us and others to be part of the region of IAPP that adopts a helical structure upon interaction with bilayer surfaces (Apostolidou, Jayasinghe, and Langen, 2008; Williamson, Loria, and Miranker, 2009). Thus, OQ_5 likely interacts with IAPP in a manner that stabilizes and/or perturbs one or more forms of its α-helical sub-domains. The NMR study supports our hypothesis that OQ_5 alters IAPP structure. Titration was limited to a stoichiometric ratio of 4:1 (OQ_5:rIAPP) as a result of limited solubility of oligoquinoline (OQ_5) at the higher IAPP concentrations required for NMR. The absence of titration sensitivity across central regions of the rIAPP sequence is not the result of mutation. A key subpeptide outside the helical subdomain of IAPP, $hIAPP_{20-29}$, was independently examined. This sub-region is the hypothesized site of amyloid nucleation, likely catalyzed by high local concentrations created by helical assembly of IAPP's N-terminal domain(Ruschak, and Miranker, 2009). The kinetic profile of 200 μM $hIAPP_{20-29}$ shows nucleation dependent kinetics with a t_{50} of 6.2±0.1 hr (Fig. 4C) consistent with previous reports assessing the independent behavior of this peptide. Inclusion of stoichiometric OQ_5 in an otherwise matched reaction results in no change in the fiber formation profile. OQ_5 inhibition of full length hIAPP at 1:1 stoichiometry (Fig. 3A) is therefore unlikely to be the result of interactions with the 20–29 sub-domain.

DISCUSSION

The development of synthetic foldamers is inspired by the capacity of proteins to fold to a conformationally restricted state, and from that state, achieve strongly specific molecular interactions (Guichard, and Huc, 2011). Oligoquinoline, a recent addition to the foldamerome (Gellman, 1998), has recently been identified by us to have the capacity to affect IAPP amyloid formation. The mechanism and effects of this interaction remained elusive. Here, we have made a series of foldamers and made comparisons both to a series of comparably derivitized protein mimetics as well as literature compounds identified through screening. Our findings show that i) OQs specifically and uniquely inhibit lipid catalyzed as well as solution phase amyloid nucleation and elongation processes, ii) perform this inhibition by interacting with a specific structural subunit of IAPP and iii), acquire these capacities in a manner that is strongly nonlinear in terms of its dependence on oligoquinoline subunit length. Our observations suggest that folded and not unfolded oligoquinolines represents the paradigm for targeting weakly ordered states IAPP.

A plethora of small molecules have previously been identified which inhibit IAPP fibrillation, e.g. polyphenols(Meng, Abedini, et al, 2010b), resveratrol(Mishra, Sellin, et al, 2009), phenolsulfonphthalein(Levy, Porat, et al, 2008), EGCG derivatives(Meng, Abedini,

et al, 2010b),acid fuchsin (Meng, Abedini, et al, 2010a), and IAPP derivatives(Yan, Tatarek-Nossol, et al, 2006). Typically, such molecules are identified using assays that measure only solution phase fibrillation. The collective result appears to be a set of molecules dominated by planar aromatic scaffolds. In the case of N-methyl derivatives of IAPP(Yan, Tatarek-Nossol, et al, 2006), the likely mechanism is not intercalation, but rather a crystal poisoning-like interaction that halts efficient elongation. In both sets of mechanisms, β-sheet structure formation represents the macromolecular target.

The capacity of OQ_5 to inhibit lipid-catalyzed assembly reflects the contribution of α-helical intermediate states to IAPP gains-of-function. Far UV-CD and NMR suggests that OQ_5 is interacting directly with the membrane bound helical sub-states of IAPP (Fig. 4) (Williamson, Loria, and Miranker, 2009). In addition, we performed assays looking for inhibition of $IAPP_{20-29}$ fibrillar assembly. This subunit assembles by direct nucleation from a random coil to a β-sheet state (Ruschak, and Miranker, 2007). No inhibition by OQ_5 was observed (Fig. 4C). Additionally, FCS data suggests that IAPP interactions with membranes are weakened by interactions with OQ_5 (Supporting Information Fig. S5). In solution, it is plausible that the inhibitory mechanism involves an alternate structure such as β-sheet. Random coil still dominates for IAPP:OQ5 in free solution potentially masking a low population of structured states (Supporting Information Fig. S6D). However, we have shown that a subset of IAPP residues weakly samples α-helical states even in the absence of membrane. Addition of a membrane model simply stabilizes this sub- population (Williamson, Loria, and Miranker, 2009). The fact that OQ_5 operates substoichiometrically for IAPP in free solution might reasonably be attributed to interactions with this small population. In total, these observations strongly support our assertion that OQ_5 interacts and affects amyloid assembly through interactions with the α-helical state of IAPP.

The adoption of a folded compact state underpins OQ capacity to affect IAPP. OQs undergo a dramatic change in their efficacy upon reaching a subunit length of five (Fig. 2E, F). This change is not accounted for by charge pairing as human IAPP contains only 2–3 positive charges. Five units is the minimum required for OQ to complete one unit of its non-covalent fold (Fig. 1). In addition, previous studies have shown that pentameric and not shorter polymers of OQ collapse into left and right handed states that do not interconvert in aqueous solution (Qi, Maurizot, et al, 2012). We therefore suggest that only at five units is OQ able to adopt the folded structure that is essential for its function.

In conclusion, a new scaffold has been identified which affects amyloid self-assembly by IAPP via a mechanism that differs from earlier reported compounds. To our knowledge, carboxylate substituted OQ_5 is the most effective IAPP self-assembly inhibitor when considering both lipid free and lipid catalyzed solution conditions. This represents a useful and new paradigm in which a folded small molecule serves to conformationally capture an off-pathway state of an intrinsically disordered peptide toxin. Indeed, this goal is central to many other systems including Aβ, α-synuclein, and others that sample a diverse set of conformational states. Oligoquinolines are a vital new class of compound to add to these important efforts.

SIGNIFICANCE

Heterogeneous disorder-to-order transitions are central to the development of cytotoxicity in many diseases including Alzheimer's, Parkinson's, and type 2 diabetes. The intrinsically disordered protein precursors in these systems lack stable secondary structure and exist as an ensemble of rapid fluctuating intermediates states. Nevertheless, they have the capacity to make structure specific interactions. Islet Amyloid Polypeptide (IAPP), a 37 residue hormonal peptide cosecreted by pancreatic β-cells samples a series of intermediate states contributing to gain of toxic function in type 2 diabetes. There are few tools, however, that can illuminate the subset of structures that give rise to any particular protein activity. A foldamer based scaffold, here based on oligoquinoline, offers an opportunity which in effect inverts the problem of molecular recognition. A designed, non-covalent interaction based on a folded and compact small molecule becomes the object about which a flexible and dynamic protein can bind. This pairing of synthetic chemistry with molecular biophysics offers a new paradigm for addressing dynamic protein targets.

Experimental Procedures

Chemical Compounds

ThT was purchased from Acros Organics (Fair Lawn, New Jersey). Lipids [dioleoylphosphatidylglycerol (DOPG) and dioleoylphosphatidylcholine (DOPC)] were purchased from Avanti Polar Lipids, Inc. (Alabaster, Al). The 96-well plates (coated, non-binding surface, black, flat bottom) were bought from Greiner Bio-One (Monroe, NC). All of the chemicals were purchased from commercial suppliers and used without further purification. Silica plates (w/UV254, aluminum backed, 200 micron) and silica gel (standard grade, particle size = 40–63 micron, 230 × 400 mesh) for flash column chromatography were purchased from Sorbent Technologies (Atlanta, GA). Dry solvents were purchased from Sigma Aldrich (St. Louis, MI) or VWR (Bridgeport, NJ). Triethylamine (dry), 2-chloro-1-methylpyridinium iodide, tert-Butyl bromoacetate, 2-nitroaniline, dimethylacetylene dicarboxylate, and polyphosphoric acid were purchased from Sigma Aldrich (St. Louis, MI).

Materials

^{15}N Wild-type rIAPP was prepared by recombinant E. coli purification as described previously (Williamson, and Miranker, 2007). Human islet amyloid polypeptide (IAPP) was synthesized by *t*-Boc methods and purified by the W. M. Keck facility (New Haven, CT). Fluorescently labeled protein was prepared using amine coupling, by reacting rIAPP with TAMRA-SE (5-carboxytetramethyl rhodamine succinimidyl ester; Life Technologies, Carlsbad, CA) for 2 h at room temperature in 10 mM potassium phosphate pH 7.2. Labeled rIAPP was separated from free dye using a HiTrap Sephadex G-25 column (GE Healthcare, Piscataway, NJ).

Synthesis of Oligoquinolines

The synthesis of oligoquinolines was carried out using linear solution phase iterative amide coupling with a slight modification in the previously reported procedure (Jiang, Lèger, and

Huc, 2003)(Jiang, Lèger, and Huc, 2003). The starting material, methyl 8-nitro-(1H)-4-quinolinone-2-carboxylate, was synthesized according to the known procedure which is then functionalized by introducing O-tert butyl ester as side chain. Chain elongation was achieved using successive amide coupling (in the presence of 2-chloro-1-methylpyridinium iodide) and reduction of nitro group. The acid labile tert-butyl ester derivatized oligoquinolines were then treated with TFA cocktail [TFA/TES/DCM (dichloromethane) (95:2.5:2.5, v/v)] to afford the carboxylate substituted oligoquinolines in modest yield. The oligquinolines were purified using HPLC and characterized for identity using NMR, MS ESI, and elemental analysis (see synthesis and characterization of oligoquinolines for details).

Preparation of IAPP

IAPP (~2 mg) was solubilized in 7 M guanidinium chloride solution. The solution was filtered (0.2 micron) and transferred to C-18 spin column, washed twice with water (400 μL each) and 10% acetonitrile in water, 0.1% formic acid (v/v) and then eluted with 200 μL of 50% acetonitrile in water, 0.1% formic acid (v/v). The concentration of IAPP (oxidized form) was calculated using absorbance measurements at 280 nm (ε = 1400 $M^{-1}cm^{-1}$). The IAPP solution was divided into several aliquots (50–100 μL, 1–2 mM), lypholized, and stored at −80°C. Fresh stock solutions of IAPP were prepared in water for each experiment.

Preparation of Unilameller Vesicles

LUVs were composed from a mixture of DOPG/DOPC in a 1:1 molar ratio. The solution of DOPG and DOPC in chloroform (25 mg/ml each) was first mixed and then dried with argon gas for 1 hr followed by drying on lyophilizer for 2 hr. The mixture was hydrated in 100 mM KCl, 50 mM sodium phosphate, and pH 7.4 for 20 minutes. A 20 mg/mL solution of lipid in buffer was passed 21 times through an extrusion film (size = 100 nm). The phospholipid content of the final material was also confirmed by measurement of total phosphorous (Chen, Toribara, and Warner, 1956).

Kinetic assay

Unless otherwise stated, kinetic reactions were conducted in buffer contains liposome (500 μg/mL) and 20 μM ThT in a Microfluor 1 black 96-well plate (Thermo Electron Corp). This was followed by addition of the small molecule dissolved in DMSO (final DMSO conc.: 0.1%, v/v). Fiber formation was initiated by addition of IAPP stock solution (final conc.:10 μM). Final volume in each well was 200 μL. The kinetics of IAPP fibrillation was monitored by ThT fluorescence (Ex 450 nm and Em 485 nm) using a FluoDia T70 fluorescence plate reader (Photon Technology International). The data were blank subtracted and renormalized to the maximum intensity of reactions containing only IAPP. All the ThT assays were performed in triplicate.

Reaction profiles were fit using the built in sigmoidal fit in Origin 5.0 separately for each run. This was used to extract separate t_{50} (time required to reach 50% fluorescence) from which average and standard deviations were calculated. All presented fits were normalized for clarity. Kinetic assays under lipid free condition were repeated in the same way as mentioned above except there was no lipid present.

Circular Dichroism spectroscopy (CD)

Circular dichroism measurements were made at room temperature on an Aviv 215 spectrometer using 1 mm path length cuvettes. The stock solution of IAPP (1–2 mM) was diluted to 30 μM IAPP in 100 mM KCl, 50 mM sodium phosphate, pH 7.4. Spectra were collected at 0.5 or 1 nm intervals from 195 to 260 nm with 10 s averaging time. The lipid catalyzed CD spectra were recorded using similar method as described above except in presence of liposome (500 mg/mL, DOPG:DOPC, 1:1, 100 nm)

Electron Microscopy (EM)

IAPP (40 μM) was incubated in buffer (100 mM KCl, 50 mM sodium phosphate, pH 7.4) both in the absence and presence of OQ_5. Aliquots of these samples were then applied on glow-discharged (25 mA and 30 sec.) carbon-coated 300-mesh copper grids for 1 min. and then dried. Grids were then negatively stained for 1 min. with uranyl acetate (2%, w/v) and dried. Micrographs of grids were examined on a Phillips Tecnai 12 transmission electron microscope at 120 kV accelerating voltages. All conclusions drawn from images in this work include at least one repeat in which the sample identity was withheld from the investigator preparing and analyzing images.

Fluorescence correlation spectroscopy (FCS)

FCS measurements were collected on a home-built instrument as previously described (Nath, Trexler, et al, 2010). Autocorrelation traces were analyzed using custom Matlab scripts.

FCS samples contained 10 nM TAMRA-labeled rIAPP in 20 mM Tris pH 7.4, 100 mM NaCl, and varying concentrations of compounds of interest added from aqueous (OQ_5) or DMSO (all other compounds, final DMSO conc.:0.5%, v/v) stocks. For IAPP-lipid binding experiments (Supporting Information Fig. S5), 5 μM of liposome (DOPG:DOPC, 1:1, 100 nm) was added to samples. Between ten and thirty 10-second measurements were averaged for each FCS observation.

All data were fit to a single-component, 3D diffusion model to extract an apparent diffusion time parameter τ_D that quantified changes in the hydrodynamic properties of IAPP:

$$G(\tau)=\frac{1}{N}\left(1+\frac{\tau}{\tau_D}\right)^{-1}\left(1+\frac{\tau}{s^2\tau_D}\right)^{-\frac{1}{2}} \quad (1)$$

Here, $G(\tau)$ represents the normalized autocorrelation at lag time τ, N represents the mean number of molecules in the observation volume, s is a structure factor that describes the prolate shape of the observation volume, and τ_D is the diffusion time.

NMR Titration

All data were collected using a Varian 600 MHz wide bore spectrometer with a triple resonance HCN probe. All experiments were performed under similar solution conditions (10% D_2O in 150 mM KCl, 50 mM sodium phosphate, pH 6.5). Titration of OQ_5 was

performed into a 120 μM ^{15}N-rIAPP sample. The dilution of rIAPP by the titration of OQ_5 was less than 6%. Reported Δ ppm values were obtained by scaling the contributions for the proton and nitrogen dimensions (Grzesiek, Stahl, et al, 1996).

Supplementary Material

Refer to Web version on PubMed Central for supplementary material.

Acknowledgments

We thank Prof Elizabeth Rhoades for useful discussions, use of custom built confocal spectrophotometer and associated expertise. We are thankful to Dr. Christopher J. Johnson and Arron B. Wolk (Mark A. Johnson's Lab, Yale University, Department of Chemistry) for FT-ICR mass spec. of oligoquinolines. This work was supported by NIH GM094693 to A.D.M.

References

Apostolidou M, Jayasinghe SA, Langen R. Structure of α-Helical Membrane-bound Human Islet Amyloid Polypeptide and Its Implications for Membrane-mediated Misfolding. Journal of Biological Chemistry. 2008; 283:17205–17210. [PubMed: 18442979]

Bieschke J, Russ J, Friedrich RP, Ehrnhoefer DE, Wobst H, Neugebauer K, Wanker EE. EGCG remodels mature a-synuclein and amyloid-β fibrils and reduces cellular toxicity. Proc Natl Acad Sci USA. 2010; 107:7710–7715. [PubMed: 20385841]

Buxbaum JN, Linke RP. A Molecular History of the Amyloidoses. J Mol Biol. 2012; 421:142–159. [PubMed: 22321796]

Cao P, Abedini A, Wang H, Tu L, Zhang X, Schmidt AM, Raleigh DP. Islet amyloid polypeptide toxicity and membrane interactions. Proceedings of the National Academy of Sciences. 2013; 110:19279–19284.

Chen PS, Toribara TY, Warner H. Microdetermination of Phosphorus. Anal Chem. 1956; 28:1756–1758.

Cummings CG, Hamilton AD. Disrupting protein–protein interactions with non-peptidic, small molecule α-helix mimetics. Curr Opin Chem Biol. 2010; 14:341–346. [PubMed: 20430687]

Gellman SH. Foldamers: A Manifesto. Acc Chem Res. 1998; 31:173–180.

Gillies ER, Dolain C, Leger J, Huc I. Amphipathic Helices from Aromatic Amino Acid Oligomers. J Org Chem. 2006; 71:7931–7939. [PubMed: 17025279]

Grzesiek S, Stahl SJ, Wingfield PT, Bax A. The CD4 Determinant for Downregulation by HIV-1 Nef Directly Binds to Nef. Mapping of the Nef Binding Surface by NMR. Biochemistry (N Y). 1996; 35:10256–10261.

Guichard G, Huc I. Synthetic foldamers. Chem Commun. 2011; 47:5933–5941.

Gurlo T, Ryazantsev S, Huang C, Yeh MW, Reber HA, Hines OJ, O'Brien TD, Glabe CG, Butler PC. Evidence for Proteotoxicity in β Cells in Type 2 Diabetes: Toxic Islet Amyloid Polypeptide Oligomers Form Intracellularly in the Secretory Pathway. The American Journal of Pathology. 2010; 176:861–869. [PubMed: 20042670]

Haataja L, Gurlo T, Huang CJ, Butler PC. Islet Amyloid in Type 2 Diabetes, and the Toxic Oligomer Hypothesis. Endocrine Reviews. 2008; 29:303–316. [PubMed: 18314421]

Hebda JA, Miranker AD. The Interplay of Catalysis and Toxicity by Amyloid Intermediates on Lipid Bilayers: Insights from Type II Diabetes. Annu Rev Biophys. 2009; 38:125–152. [PubMed: 19416063]

Hebda JA, Saraogi I, Magzoub M, Hamilton AD, Miranker AD. A Peptidomimetic Approach to Targeting Pre-amyloidogenic States in Type II Diabetes. Chem Biol. 2009; 16:943–950. [PubMed: 19778722]

Jiang H, Lèger J, Huc I. Aromatic δ-Peptides. J Am Chem Soc. 2003; 125:3448–3449. [PubMed: 12643704]

Kumar S, Miranker AD. A foldamer approach to targeting membrane bound helical states of islet amyloid polypeptide. Chem Commun. 2013; 49:4749–4751.

Levy M, Porat Y, Bacharach E, Shalev DE, Gazit E. Phenolsulfonphthalein, but Not Phenolphthalein, Inhibits Amyloid Fibril Formation: Implications for the Modulation of Amyloid Self-Assembly. Biochemistry (N Y). 2008; 47:5896–5904.

Magzoub M, Miranker AD. Concentration-dependent transitions govern the subcellular localization of islet amyloid polypeptide. FASEB J. 2012; 26:1228–1238. [PubMed: 22183778]

Meng F, Abedini A, Plesner A, Middleton CT, Potter KJ, Zanni MT, Verchere CB, Raleigh DP. The Sulfated Triphenyl Methane Derivative Acid Fuchsin Is a Potent Inhibitor of Amyloid Formation by Human Islet Amyloid Polypeptide and Protects against the Toxic Effects of Amyloid Formation. J Mol Biol. 2010a; 400:555–566. [PubMed: 20452363]

Meng F, Abedini A, Plesner A, Verchere CB, Raleigh DP. The Flavanol (−)-Epigallocatechin 3-Gallate Inhibits Amyloid Formation by Islet Amyloid Polypeptide, Disaggregates Amyloid Fibrils, and Protects Cultured Cells against IAPP-Induced Toxicity. Biochemistry (N Y). 2010b; 49:8127–8133.

Mishra R, Sellin D, Radovan D, Gohlke A, Winter R. Inhibiting Islet Amyloid Polypeptide Fibril Formation by the Red Wine Compound Resveratrol. ChemBioChem. 2009; 10:445–449. [PubMed: 19165839]

Nath, A.; Trexler, AJ.; Koo, P.; Miranker, AD.; Atkins, WM.; Rhoades, E. Methods in Enzymology. Academic Press; 2010. Chapter 6 - Single-Molecule Fluorescence Spectroscopy Using Phospholipid Bilayer Nanodiscs; p. 89-117.

Qi T, Maurizot V, Noguchi H, Charoenraks T, Kauffmann B, Takafuji M, Ihara H, Huc I. Solvent dependence of helix stability in aromatic oligoamide foldamers. Chem Commun. 2012; 48:6337–6339.

Ruschak AM, Miranker AD. The Role of Prefibrillar Structures in the Assembly of a Peptide Amyloid. J Mol Biol. 2009; 393:214–226. [PubMed: 19524594]

Ruschak AM, Miranker AD. Fiber-dependent amyloid formation as catalysis of an existing reaction pathway. Proc Natl Acad Sci USA. 2007; 104:12341–12346. [PubMed: 17640888]

Walsh DM, Klyubin I, Fadeeva JV, Cullen WK, Anwyl R, Wolfe MS, Rowan MJ, Selkoe DJ. Naturally secreted oligomers of amyloid beta] protein potently inhibit hippocampal long-term potentiation in vivo. Nature. 2002; 416:535–539. [PubMed: 11932745]

Williamson JA, Loria JP, Miranker AD. Helix Stabilization Precedes Aqueous and Bilayer-Catalyzed Fiber Formation in Islet Amyloid Polypeptide. J Mol Biol. 2009; 393:383–396. [PubMed: 19647750]

Williamson JA, Miranker AD. Direct detection of transient alpha-helical states in islet amyloid polypeptide. Protein Science. 2007; 16:110–117. [PubMed: 17123962]

Winner B, Jappelli R, Maji SK, Desplats PA, Boyer L, Aigner S, Hetzer C, Loher T, Vilar M, Campioni S, et al. In vivo demonstration that a-synuclein oligomers are toxic. Proceedings of the National Academy of Sciences. 2011; 108:4194–4199.

Wolfe LS, Calabrese MF, Nath A, Blaho DV, Miranker AD, Xiong Y. Protein-induced photophysical changes to the amyloid indicator dye thioflavin T. Proc Natl Acad Sci USA. 2010; 107:16863–16868. [PubMed: 20826442]

Yan L, Tatarek-Nossol M, Velkova A, Kazantzis A, Kapurniotu A. Design of a mimic of nonamyloidogenic and bioactive human islet amyloid polypeptide (IAPP) as nanomolar affinity inhibitor of IAPP cytotoxic fibrillogenesis. Proc Natl Acad Sci USA. 2006; 103:2046–2051. [PubMed: 16467158]

HIGHLIGHTS

- Oligoquinolines fold in water to a compact state with a derivitizable exterior
- The disordered precursor of diabetic amyloid is inactivated by this scaffold
- Inactivation is uniquely mediated in aqueous and bilayer milieus
- Imposing structure on a disordered protein is a new way to manipulate its function

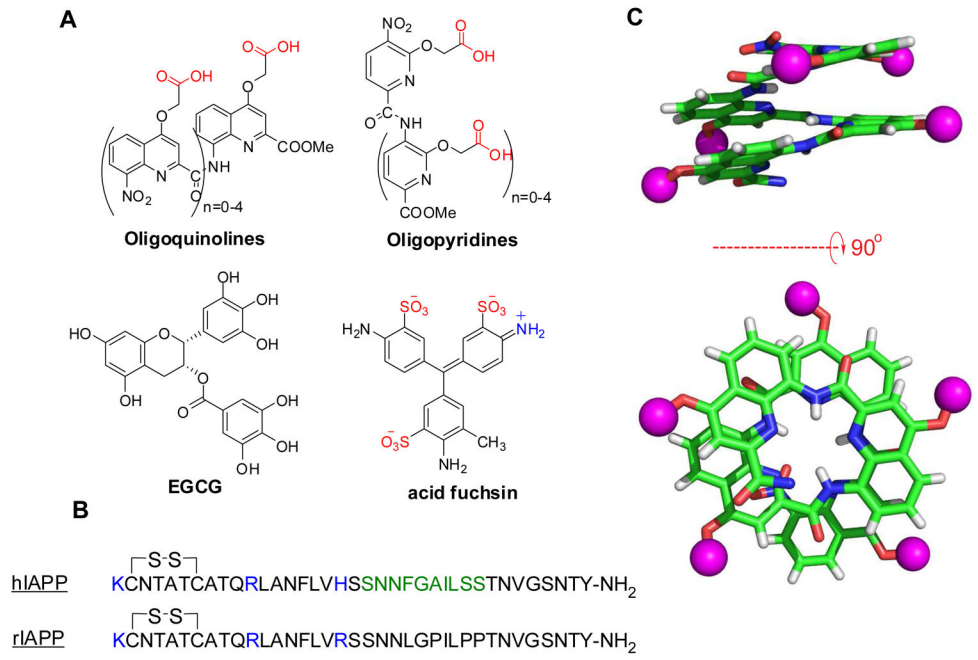

Figure 1.

Chemical structures used in this study. (A, B) Line drawings of small molecules and primary sequences of human and rat variants of IAPP. IAPP contains the indicated disulfide bond and is post-translationally amidated at its C-terminus. A subdomain spanning residues 20–29, $IAPP_{20\text{-}29}$, is shown in green. (C) Pentameric oligoquinalone adapted from the crystal structure of a larger polymer(Gillies, Dolain, et al, 2006). The magenta spheres are substitutable R-groups, which for OQ_5, are COOH.

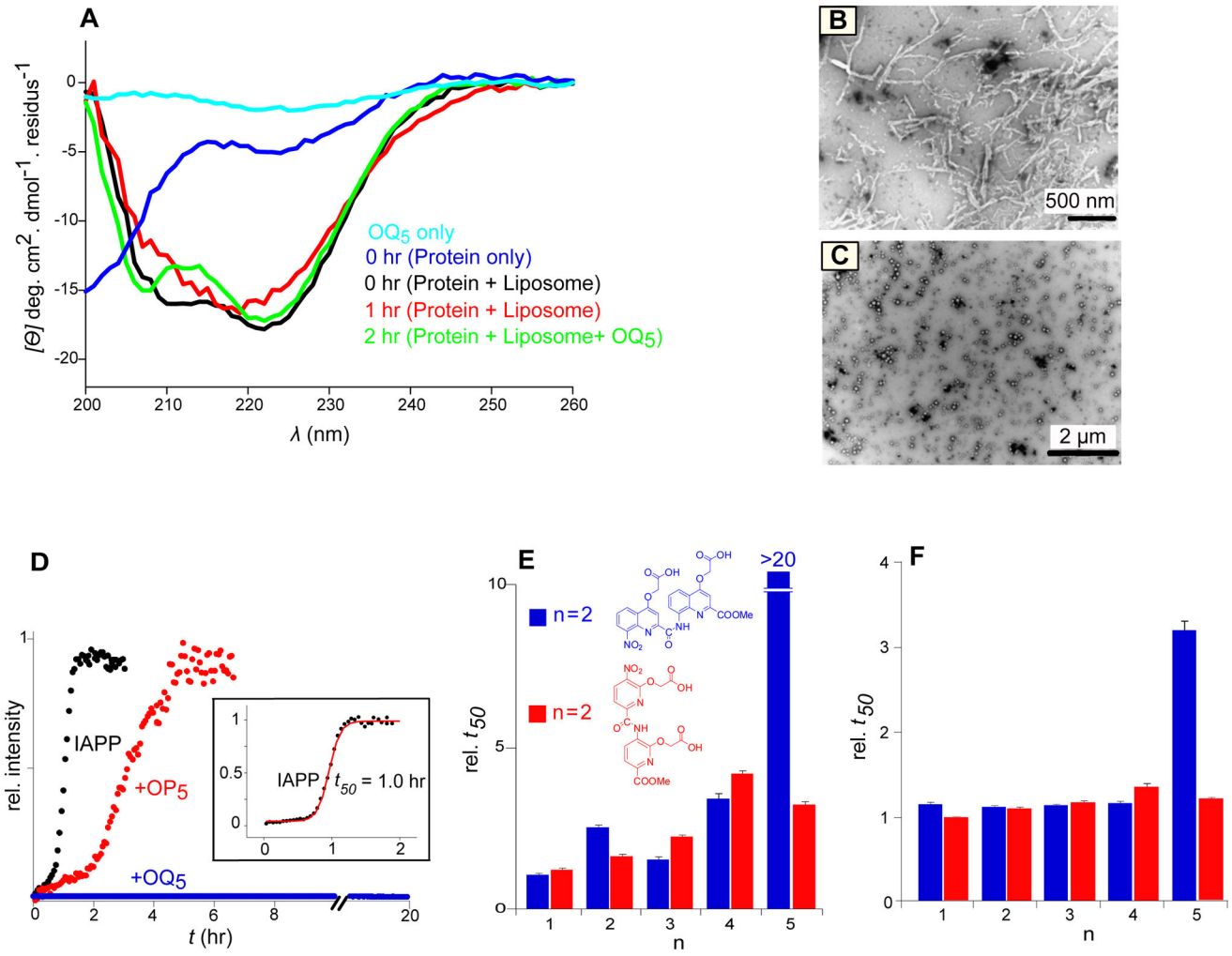

Figure 2.

Effect of alternative ligands on lipid catalyzed IAPP fibrillation. (A) CD spectra of 30μM IAPP in presence and absence of 630 μM (monomer units) unilamellar liposomes and/or 30 μM OQ_5. (B) Negative stain, TEM images of 10 μM IAPP incubated in reaction buffer for 2 hr in the presence (C) or absence (B) of 10 μM OQ_5. (D) Representative kinetic profiles of 10 μM IAPP fibrillation initiated in the absence and presence of 100 μM ligands and detected by changes in the intensity of an indicator fluorophore (see methods). (Inset) A sigmoidal fit is used to determine the time required to reach 50% conversion, t_{50}. (E, F) A comparison of the relative t_{50} of 10 μM IAPP fibrillation by 100 μM (E) and 10 μM (F) of oligoquinolines (blue) and oligopyridyls (red). The reported t_{50} values were calculated from sigmoidal fit using Origin 5.0 from three independent experiments with margin of error reported as SD.

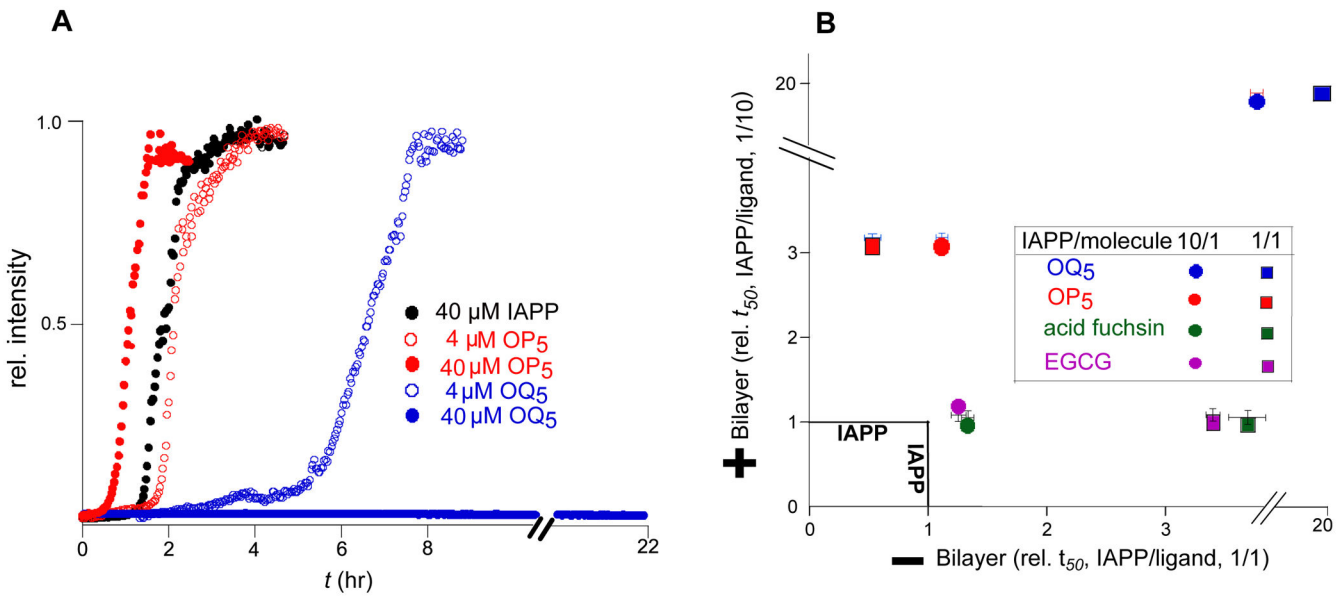

Figure 3.

Comparison of the effect of alternative ligands on IAPP fibrillation. Reaction profiles shown at stoichiometric ratios of 1:1 (filled) and 1:10 (open) (small molecule:IAPP). (A) Kinetic assays were performed at 40 μM IAPP in the absence of LUVs. Representative profiles are shown for OQ_5 and OP_5 only. (B) Comparison of ligand activity towards 40 and 10 μM of IAPP fibrillation, under lipid-free and lipid-catalyzed conditions respectively. All t_{50} are expressed as t_{50} in the presence of compound divided by the t_{50} of a compound free control reaction. The reported t_{50} values were calculated from sigmoidal fit using Origin 5.0 from three independent experiments with margin of error reported as SD.

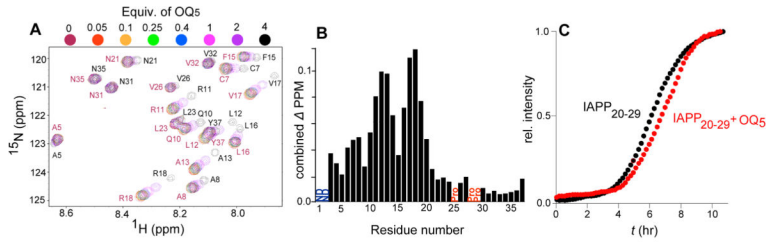

Figure 4.

(A) Overlay of the changes in chemical shifts in ^{1}H-^{15}N HSQC NMR spectra of 120 μM ^{15}N-labelled rIAPP titrated with OQ_5 at the indicated stoichiometries. (B) Sequence dependence of combined $^{15}N/^{1}H$ chemical shifts at a stoichiometric ratio of 4:1 (OQ_5:IAPP) (Grzesiek, Stahl, et al, 1996). (C) Effect of equimolar OQ_5 on the kinetic profile of 200 μM $hIAPP_{20\text{-}29}$ fibrillation.